

MULTIRESOLUTION REPRESENTATION IN UNSTRUCTURED MESHES*

RÉMI ABGRALL[†] AND AMI HARTEN[‡]

Abstract. In this paper we describe techniques to represent data which originate from discretization of functions in unstructured meshes in terms of their *local* scale components. To do so we consider a nested sequence of discretization, which corresponds to increasing levels of resolution, and we define the scales as the “difference in information” between any two successive levels. We obtain data compression by eliminating scale-coefficients which are sufficiently small. This capability for data compression can be used to reduce the cost of numerical schemes by solving for the more compact representation of the numerical solution in terms of its significant scale-coefficients.

Key words. multiresolution analysis, unstructured meshes, ENO reconstruction

AMS subject classifications. 65D99, 65M99, 41A05

PII. S0036142997315056

1. Introduction. Fourier analysis, which provides a way to represent square-integrable functions in terms of their sinusoidal scale-components, has contributed greatly to all fields of science. The main drawback of Fourier analysis is in its globality; a single irregularity in the function dominates the behavior of the scale-coefficients and prevents us from getting immediate information about the behavior of the function elsewhere.

The recent development of the theory of wavelets (see [18] and [17]) was a great step towards local scale decomposition, and has already had great impact on several fields of science. In numerical analysis, representation by compactly supported wavelets (see [8] and [7]) is used to reduce the cost of many numerical solution algorithms (see [4]). The main drawback of the theory of wavelets is that it decomposes any square integrable function into scale-components which are translates and dilates of a *single* function. Consequently there are conceptual difficulties in extending wavelets to bounded domains and general geometries.

In [10, 13] we introduced the concept of “nested discretization,” which enables us to represent data that originates from unstructured grids in bounded domains in terms of its scale decomposition. This framework is a generalization of the theory of wavelets in the sense that under conditions of uniformity its natural result is wavelets.

The main application of this new capability is to the numerical solution of partial differential equations in complex geometries, e.g., the solution of the equations of compressible gas around an airplane. As we have demonstrated in a series of articles on multiresolution schemes for the solution of hyperbolic conservation laws in Cartesian grids (see [12, 11] and [6, 5]), there is a lot to be gained by formulating the time-evolution of the problem in terms of the more compact representation of the solution

*Received by the editors January 15, 1997; accepted for publication (in revised form) September 25, 1997; published electronically November 13, 1998.

<http://www.siam.org/journals/sinum/35-6/31505.html>

[†]Mathématiques Appliquées de de Bordeaux, Université de Bordeaux I, 351 Cours de la Libération, 33 405 Talence Cedex, France (abgrall@math.u-bordeaux.fr). The research of this author was supported by National Science Foundation grant DMS91-03104 and NATO grant 1/B/93/France during his stay at the Department of Mathematics, University of California, Los Angeles, CA.

[‡]The author is deceased. Former address: School of Mathematical Sciences, Tel-Aviv University, Tel-Aviv, Israel. The research of this author was supported by Office of Naval Research grant N00014-92-J-1890 and National Science Foundation grant DMS91-03104.

by its significant scale-coefficients. This technique is an attractive alternative to the methodology of adaptive grids, and it enables us to dynamically adjust the local level of resolution to the variation of the solution.

Unstructured meshes have been used primarily for two purposes: (1) to have a faithful description of the boundary in order to accurately impose the boundary conditions which determine the solution; (2) to serve as an implementation of adaptive grid ideas. Unfortunately the computation of numerical solutions on unstructured grids is considerably more expensive than that on Cartesian grids. Since we can accomplish the adaptivity part by using multiresolution schemes on uniform grids, what remains is the use of unstructured meshes to describe the geometry of the boundary. In the future, we plan to use a relatively thin layer of unstructured mesh around the airplane and to switch to a more regular grid further away. In [2] we present preliminary results on multiresolution schemes for hyperbolic conservation laws on unstructured grids.

In the present paper, we describe multiresolution representation (MR) schemes for data which are obtained by discretization of functions in unstructured meshes either by taking point values at the “nodes” or by taking averages over the “cells” of the mesh. We pay special attention to the description of the boundary of the domain in the process of coarsening/refinement which is associated with generating the various levels of resolution.

Since the preliminary version of this paper [3] has been written, several authors have developed algorithms to allow multiresolution analysis on unstructured meshes. One may mention the “lifting schemes” of Sweldens [22] which allow definition of biorthogonal decompositions in the setting of unstructured grids (see [20] for applications to image processing). Hierarchical finite elements wavelet basis have been constructed by Oswald and Lorenz [19] and Stevenson [21]. These algorithms work on structured triangulation. As the situation is rather different than in the present paper, they can push the analysis much farther.

2. General framework for MR. In this section we describe the abstract general framework for MR of data. We consider discrete data which is associated with a nested sequence of discretization $\{\mathcal{D}_k\}_{k=0}^L$ and show how to design schemes for its MR. Later we shall apply this general framework to data which correspond to discretization of functions in unstructured grids.

DEFINITION 2.1. *Let \mathcal{F} be a vector space and $(V_k)_{k=0}^\infty$ be a sequence of finite dimensional vector spaces, $\dim V_k = J_k$. We say that a sequence of linear operators $\{\mathcal{D}_k\}_{k=0}^\infty$, $\mathcal{D}_k : \mathcal{F} \rightarrow V^k$, is a nested sequence of discretization if for any $k = 0, \dots, +\infty$,*

1. \mathcal{D}_k is onto,
2. the null spaces satisfy $\mathcal{N}(\mathcal{D}_k) \subset \mathcal{N}(\mathcal{D}_{k+1})$.

In the following we show how to obtain MR of any discrete data $v^L = \mathcal{D}_L f$, where the scale-decomposition corresponds to the levels of resolution which are introduced in Definition 2.1. This is a very general framework which allows for discretizations corresponding to unstructured grids in several space dimensions.

First we show that a nested sequence of discretization comes equipped with a decimation operator D_k^{k-1} , which is a linear mapping from $V^k = \mathcal{D}_k(\mathcal{F})$ onto $V^{k-1} = \mathcal{D}_{k-1}(\mathcal{F})$:

$$(2.1) \quad D_k^{k-1} : V^k \xrightarrow{\text{onto}} V^{k-1}.$$

This decimation operator is defined as follows. For any v in V^k there is at least one $f \in \mathcal{F}$ such that $\mathcal{D}_k f = v$; the decimation of v is $\mathcal{D}_{k-1} f \in V^{k-1}$, i.e.,

$$(2.2) \quad v \in V^k, \quad v = \mathcal{D}_k f, \quad D_k^{k-1} v = \mathcal{D}_{k-1} f.$$

It follows from Definition 2.1 that D_k^{k-1} is well defined by (2.2); i.e., its definition is independent of the particular f .

Given $v^L \in V^L$, we can evaluate $\{v^k\}_{k=0}^{L-1}$ by repeated decimation

$$(2.3) \quad v^{k-1} = D_k^{k-1} v^k, \quad k = L, \dots, 1.$$

Since (2.2) implies that

$$(2.4) \quad D_k^{k-1}(\mathcal{D}_k f) = \mathcal{D}_{k-1} f \quad \text{for any } f \in \mathcal{F},$$

we get for any $f \in \mathcal{F}$ for which $v^L = \mathcal{D}_L f$, that $v^k = \mathcal{D}_k f$ for all k in (2.3). We would like to stress the point that this decimation is done without explicit knowledge of f .

Since by Definition 2.1 $V^k = \mathcal{D}_k(\mathcal{F})$, it follows that \mathcal{D}_k has a right-inverse (at least one), which we denote by \mathcal{R}_k :

$$(2.5) \quad \mathcal{R}_k : V^k \rightarrow \mathcal{F}, \quad \mathcal{D}_k \mathcal{R}_k = I_k,$$

where I_k denotes the identity operator in V^k . Since $(\mathcal{R}_k v^k) \in \mathcal{F}$ is an approximation to any $f \in \mathcal{F}$ for which $\mathcal{D}_k f = v^k$, we refer to \mathcal{R}_k as a reconstruction of \mathcal{D}_k .

Next we show that any sequence of corresponding reconstruction operators $\{\mathcal{R}_k\}_{k=0}^L$ defines an MR scheme for discrete data v^L in V^L . Starting from v^{k-1} in (2.3) we can get an approximation to v^k by

$$(2.6) \quad v^k \approx \mathcal{D}_k(\mathcal{R}_{k-1} v^{k-1}).$$

We denote

$$P_{k-1}^k =: \mathcal{D}_k \mathcal{R}_{k-1}, \quad P_{k-1}^k : V^{k-1} \rightarrow V^k$$

and refer to it as prediction operator. It follows immediately from taking $f = \mathcal{R}_{k-1} v^{k-1}$ in (2.4) and using (2.5) that P_{k-1}^k is a right-inverse of the decimation D_k^{k-1} :

$$D_k^{k-1} P_{k-1}^k = I_{k-1}.$$

We observe that the prediction error e^k ,

$$(2.7) \quad e^k = v^k - P_{k-1}^k v^{k-1} = (I_k - P_{k-1}^k D_k^{k-1}) v^k,$$

satisfies the relation

$$D_k^{k-1} e^k = D_k^{k-1} v^k - (D_k^{k-1} P_{k-1}^k) v^{k-1} = v^{k-1} - v^{k-1} = 0,$$

and therefore it is in the null space of the decimation operator

$$e^k \in \mathcal{N}(D_k^{k-1}) = \{v \mid v \in V^k, D_k^{k-1} v = 0\}.$$

It follows from (2.1) that

$$\dim \mathcal{N}(D_k^{k-1}) = J_k - J_{k-1},$$

and therefore the prediction error e^k , which is described in terms of J_k components in V^k , can be represented by $(J_k - J_{k-1})$ scale-coefficients $d^k = \{d_j^k\}_{j=1}^{J_k - J_{k-1}}$. Specifically, let $\{\mu_j^k\}_{j=1}^{J_k - J_{k-1}}$ be any basis of $\mathcal{N}(D_k^{k-1})$,

$$\mathcal{N}(D_k^{k-1}) = \text{span}\{\mu_j^k\}_{j=1}^{J_k - J_{k-1}},$$

and let d^k denote the coordinates of e^k in this basis:

$$e^k = \sum_{j=1}^{J_k - J_{k-1}} d_j^k \mu_j^k =: E_k d^k, \quad d^k =: G_k e^k.$$

Here G_k denotes the operator which assigns to $e^k \in \mathcal{N}(D_k^{k-1})$ its coordinates d^k in the basis $\{\mu_j^k\}_{j=1}^{J_k - J_{k-1}}$; observe that $E_k G_k$ is the projection operator onto $\mathcal{N}(D_k^{k-1})$.

Next we show that there is a one-to-one correspondence between v^k and $\{d^k, v^{k-1}\}$. Given v^k , we evaluate

$$\begin{cases} v^{k-1} &= D_k^{k-1} v^k, \\ d^k &= G_k (I_k - P_{k-1}^k D_k^{k-1}) v^k; \end{cases}$$

given v^{k-1} and d^k , we recover v^k by

$$\begin{aligned} P_{k-1}^k v^{k-1} + E_k d^k &= P_{k-1}^k D_k^{k-1} v^k + E_k G_k (I_k - P_{k-1}^k D_k^{k-1}) v^k \\ &= P_{k-1}^k D_k^{k-1} v^k + (I_k - P_{k-1}^k D_k^{k-1}) v^k \\ &= v^k. \end{aligned}$$

Applying the above for $k = L, \dots, 1$, we get that

$$v^L \xleftrightarrow{1:1} \{d^L, \dots, d^1, v^0\} =: \hat{v}_M;$$

we refer to \hat{v}_M as the MR of v^L .

The direct MR transform $\hat{v}_M = M \cdot v^L$ is given by the algorithm

$$(2.8) \quad \begin{cases} \text{Do } k = L, \dots, 1, \\ v^{k-1} = D_k^{k-1} v^k, \\ d^k = G_k (I_k - P_{k-1}^k D_k^{k-1}) v^k =: G_k^D v^k. \end{cases}$$

The inverse MR transform $v^L = M^{-1} \cdot \hat{v}_M$ is given by

$$\begin{cases} \text{Do } k = 1, \dots, L, \\ v^k = P_{k-1}^k v^{k-1} + E_k d^k. \end{cases}$$

We remark that in multigrid terminology, D_k^{k-1} is “restriction” and P_{k-1}^k is “prolongation.” In signal processing, D_k^{k-1} plays the role of “low-pass filter” while G_k^D , which is defined in (2.8), plays the role of “high-pass filter.”

In order to apply this MR to real-life problems for purposes of analysis and data compression, we have to make sure that the direct MR transform and its inverse are stable with respect to perturbations. In [13], we present stability analysis for MR schemes through the different scales and derive a sufficient condition which seems to be “close” to necessary; this condition also implies existence of a multiresolution basis for functions in \mathcal{F} . In Appendix B, we review some elements of this analysis and relate them to the particular examples of the present paper.

In the following we describe techniques to generate a nested sequence of discretization which corresponds to unstructured meshes in \mathbb{R}^m , and present specific algorithms for \mathbb{R}^2 . The main application of this methodology is to the numerical solution of PDEs in complex geometries. Our basic approach to this application is that “the user” should provide a mesh and an appropriate numerical method, and we assume that he is satisfied with the quality of these numerical results; furthermore, we assume that the solution is overresolved in large parts of the computational domain (this may be due to propagation in time of existing regions of large variation or due to the natural laziness of a “user”). Our task is to provide an MR scheme which will enable us to calculate these same results, within a user-supplied tolerance for error but in a much faster way, by performing the computation in the suitable local level of resolution. To do so we apply a coarsening procedure to the given mesh to generate a *nested* sequence of discretization, and find an appropriate sequence of reconstruction operators. Once this is accomplished we use the machinery of this section to obtain multiresolution representation of data in the user-supplied mesh. We remark that the preliminary results of applying this program to hyperbolic conservation laws are encouraging (see [12, 11, 6, 5]).

A more ambitious program is to endow the MR scheme with the capability to increase the level of resolution above that of the user-supplied mesh if the analysis of the scale coefficients indicates the need to do so due to development of large variation on a smaller scale (of course the user has to supply a limit on the smallest scale that he is willing to pay for). At present we are not doing that, and therefore the main interest in this paper is in developing coarsening procedures that result in a sequence of nested discretization; however, we shall also consider the question of refinement. We would like to point out again that the main use of unstructured grids is for the geometry of the problem, and thus in both coarsening and refinement, one has to pay special attention to the boundaries and make sure that they are appropriately resolved.

In this report, we present some numerical experiments of data compression in unstructured meshes and compare them to similar experiments with MR schemes for uniform tensor-product grids (which are known to be stable). These experiments indicate that, in spite of the strong nonuniformity in our unstructured meshes, the compression ratio and the compression error are of the same order as those of the uniform tensor-product grids.

3. MR schemes for point value discretization. Consider bounded functions $f \in \mathcal{F}$,

$$f : \Omega \subset \mathbb{R}^m \longrightarrow \mathbb{R}, \quad \mathcal{F} = \mathcal{B}(\Omega),$$

where Ω is a bounded domain; take any sequence

$$(3.1) \quad X^k = \{x_i^k\}_{i=0}^{J_k}, \quad x_i^k \in \Omega;$$

and define $v^k = \mathcal{D}_k f$ by

$$(3.2) \quad v_i^k = (\mathcal{D}_k f)_i = f(x_i^k), \quad v^k = \{v_i^k\}_{i=0}^{J_k}.$$

We refer to (3.1)–(3.2) as discretization by point value. Note that here the index starts from $i = 0$, and thus there are $J_k + 1$ elements in X^k .

The sequence of discretization $\{\mathcal{D}_k\}$ in (3.1)–(3.2) is nested if and only if for all k

$$X^{k-1} \subset X^k;$$

decimation in this case amounts to removing from v^k components $v_i^k = f(x_i^k)$ for $x_i^k \notin X^{k-1}$. Note that the decimation operator D_k^{k-1} is defined directly from the sequence $\{\mathcal{D}_k\}$.

Let $\mathcal{I}_k(x; v^k)$ denote *any* interpolation of $\{v_i^k\}$ at the corresponding nodes $\{x_i^k\}$, i.e.,

$$(3.3) \quad \mathcal{I}_k(x_i^k; v^k) = v_i^k \quad \text{for all } x_i^k \in X^k,$$

and observe that

$$(3.4) \quad \mathcal{D}_k \mathcal{I}_k(\cdot; v^k) = v^k.$$

The above relation shows that reconstruction in this case amounts to a selection of an interpolation technique in (3.3). Given v^{k-1} we approximate v^k by (2.6), and get the prediction error e^k (2.7),

$$e_i^k = v_i^k - \mathcal{I}_{k-1}(x_i^k; v^{k-1}) \quad \text{for all } x_i^k \in X^k.$$

Using multigrid terminology, this prediction can be expressed by saying that we use injection of the values corresponding to x_i^k which are in X^{k-1} and interpolation for those which are not in X^{k-1} . Observe that the prediction error $e_i^k = 0$ for all i such that $x_i^k \in X^{k-1}$. We define the scale-coefficients $d^k = \{d_j^k\}$ as the prediction error in $X^k - X^{k-1}$, i.e.,

$$d_j^k = e_{i_j}^k \quad \text{for all } x_{i_j}^k \notin X^{k-1},$$

where i_j for $j = 1, \dots, (J_k - J_{k-1})$ is some ordering of the points in $X^k - X^{k-1}$:

$$(3.5) \quad \{x_{i_j}^k\}_{j=1}^{J_k - J_{k-1}} = X^k - X^{k-1}.$$

Example 3.1. Triangulation in \mathbb{R}^2 . As a result of the success of the finite element method for the numerical solution of PDEs, we have many triangulation techniques (some of them are packaged as computer codes) to construct a mesh of desired resolution with a good description of the boundary for complex geometries, and also corresponding interpolation methods for the nodes. Let us denote the triangles in such a mesh by $T_i^k \subseteq \Omega$, $1 \leq i \leq n_t$, and denote by X^k the set of vertices in these triangles; we refer to $\mathcal{T}^k =: \{T_i^k\}_{i=1}^{n_t}$ as the triangulation of Ω . Observe that $\Omega^k =: \cup_{i=1}^{n_t} T_i^k \subseteq \Omega$ is a polygon and that $\partial\Omega^k$ is a piecewise-linear approximation to $\partial\Omega$.

In our particular application, we are interested in local approximations. Once the discretization operators are defined, the only degree of freedom left is the choice of the reconstruction operators. For this purpose we use the following piecewise-polynomial

interpolation. Let \mathcal{S}_i^k be a stencil of $s = r(r + 1)/2$ points of X^k which is assigned to the triangle $T_i^k \in \mathcal{T}^k$ and includes its vertices. Let $p_i^k(x; \mathcal{D}_k f)$ denote the unique polynomial of degree $(r - 1)$ for $r \geq 2$ which interpolates $f(x)$ at the points of the stencil \mathcal{S}_i^k , and define

$$(3.6) \quad \mathcal{I}_k(x; \mathcal{D}_k f) = p_i^k(x; \mathcal{D}_k f) \text{ for } x \in T_i^k.$$

Clearly this technique is exact for data of polynomial functions of degree less or equal to $r - 1$. Observe, however, that unlike 1D, \mathcal{I}_k is not necessarily continuous on the boundary of T_i^k ; in this case, we take \mathcal{F} to be the space $\mathcal{B}(\Omega)$ with the sup norm rather than $C^0(\Omega)$.

For $r = 2$, the 3 points of \mathcal{S}_i^k are necessarily the vertices of T_i^k , and $p_i^k(x; \mathcal{D}_k f)$ is the piecewise-linear function which interpolates f at these three points. Observe that in this case, $\{\mathcal{I}_k(x; \mathcal{D}_k f)\}$ is a sequence of continuous functions which forms a hierarchic sequence of approximation in $C^0(\Omega)$.

For $r > 2$, we have several reasonable choices of stencils; one can use this freedom to adapt the interpolation to the nature of the data by choosing the stencil in which the data is smoothest, and thus avoid the Gibbs' phenomenon (see [1] and [14]).

In Appendix A, we describe a simple strategy to select a "centered" stencil of six vertices for piecewise-quadratic interpolation ($r = 3$).

Our main problem is to design procedures for coarsening and refinement for which the vertices of \mathcal{T}^{k-1} are contained in those of \mathcal{T}^k . The design of such procedures (in the case $r = 3$) is the topic of section A.

4. MR schemes for cell-average discretization. Consider absolutely integrable functions $f \in \mathcal{F}$,

$$f : \Omega \subset \mathbb{R}^m \longrightarrow \mathbb{R}, \quad \mathcal{F} = L^1(\Omega),$$

where Ω is a compact set, and let $\mathcal{C}^k = \{C_i^k\}_{i=1}^{J_k}$ be a set of cells such that

$$\Omega^k =: \overline{\cup_{i=1}^{J_k} C_i^k} \subseteq \Omega, \quad C_i^k \cap C_j^k = \emptyset \text{ for } i \neq j.$$

We define the cell-average discretization of f by

$$(\mathcal{D}_k f)_i = \frac{1}{|C_i^k|} \int_{C_i^k} f(x) dx, \quad |C_i^k| = \int_{C_i^k} dx.$$

Next let us consider a refinement sequence $\{\mathcal{C}^k\}_{k=0}^L$, in which \mathcal{C}^k is formed from \mathcal{C}^{k-1} by dividing each cell C_i^{k-1} into, say q , disjoint cells $\{C_{i_\ell}^k\}_{\ell=1}^q$,

$$(4.1) \quad \overline{\cup_{\ell=1}^q C_{i_\ell}^k} = \overline{C_i^{k-1}}.$$

Alternatively, we can consider (4.1) to be a coarsening procedure in which we agglomerate every q cells of \mathcal{C}^k into a larger cell of \mathcal{C}^{k-1} ; the only reason that we take here a fixed q is to simplify the notations. In any case, the sequence of discretization $\{\mathcal{D}_k\}_{k=0}^L$ is nested, and it follows from the additivity of the integral that

$$(\mathcal{D}_{k-1} f)_i = \frac{1}{|C_i^{k-1}|} \sum_{\ell=1}^q |C_{i_\ell}^k| (\mathcal{D}_k f)_{i_\ell} = (\mathcal{D}_k^{k-1} \mathcal{D}_k f)_i,$$

which directly defines the decimation operator in (2.1)–(2.2). Let \mathcal{R}_k denote any reconstruction from cell-averages, linear or not, and let e^k denote the prediction error

in (2.7). In this particular example, e^k is defined by the local errors e_i^k on the cells C_i^k . Since $e^k \in \mathcal{N}(D_k^{k-1})$, we have in this particular case

$$(4.2) \quad \sum_{\ell=1}^q |C_{i_\ell}^k| e_{i_\ell}^k = 0.$$

This relation shows that we can define the scale-coefficients d^k by taking $(q - 1)$ properly chosen linear combinations of the q prediction errors $\{e_{i_\ell}^k\}_{\ell=1}^q$ in each cell C_i^{k-1} . These linear combinations should be chosen so that together with (4.2) they constitute an invertible system of q linear equations for the prediction errors $\{e_{i_\ell}^k\}_{\ell=1}^q$ in the cell C_i^{k-1} (e.g., see [15] for such combinations in representation of matrices).

Example 4.1. Unstructured meshes in \mathbb{R}^m . Using agglomeration as a coarsening technique may result in cells which are general polygons. As in section 3, the only degree of freedom left is the reconstruction. As before, we are interested in local approximations. In the following, we describe a piecewise-polynomial reconstruction technique which is suitable for our purpose (see [14]). Let us denote by \mathcal{S}_i^k a stencil of $s(r)$ cells in \mathcal{C}^k which includes C_i^k , i.e.,

$$(4.3) \quad \mathcal{S}_i^k = \{C_{i_m}^k\}_{m=1}^{s(r)}, \quad C_i^k \in \mathcal{S}_i^k.$$

Here $s(r)$ is the number of coefficients in a polynomial of degree $(r - 1)$ in \mathbb{R}^m . Let $p_i^k(x; \mathcal{D}_k f)$ denote the unique polynomial of degree $(r - 1)$ which attains the averages $(\mathcal{D}_k f)_{i_m}$ in \mathcal{S}_i^k , i.e., the one which satisfies the system of $s(r)$ linear equations for its $s(r)$ coefficients,

$$(4.4) \quad \frac{1}{|C_{i_m}^k|} \int_{C_{i_m}^k} p_i^k(x; \mathcal{D}_k f) dx = (\mathcal{D}_k f)_{i_m}, \quad m = 1, \dots, s(r),$$

and define

$$(4.5) \quad (\mathcal{R}_k \mathcal{D}_k f)(x) = p_i^k(x; \mathcal{D}_k f) \quad \text{for } x \in C_i^k.$$

Clearly (4.3)–(4.5) define a reconstruction of $\mathcal{D}_k f$ which is exact for polynomial functions of degree less than or equal to $(r - 1)$ and thus is r th order accurate. Such a polynomial exists if (a) $s(r) = r(r + 1)/2$ and (b) a Vandermonde-type condition on \mathcal{S}_i^k is satisfied.

A general discussion on this kind of polynomial approximation and its computation appears in [1] and [14]. In the following, we always assume that the stencils we construct are admissible. In practice, there is no particular restriction, (see [1]).

Note that for $r = 1$ in (4.3)–(4.5), we have $s(r) = 1$ and we get the piecewise-constant reconstruction

$$(\mathcal{R}_k \mathcal{D}_k f)(x) = \sum_i (\mathcal{D}_k f)_i \chi_{C_i^k}(x),$$

where $\chi_C(x)$ denotes the characteristic function of the set C ,

$$\chi_C(x) = \begin{cases} 1, & x \in C, \\ 0, & \text{otherwise.} \end{cases}$$

In [14], we present a hierarchial algorithm for the selection of a “centered” stencil, which is applicable even to completely unstructured meshes in \mathbb{R}^m . In this context

the “centered” stencil is defined as the one which minimizes the reconstruction error for the one-higher degree polynomials (i.e., degree r). This algorithm is of “crystal growth” type: starting with the cell C_i^k , we begin to add successively, one cell at a time, to the cluster of cells that we have at the beginning of each step. The cell which is being added is selected from the set of all side-neighbors of the existing cluster by the requirement that it will minimize the reconstruction error of suitably chosen monomials.

In [14], we also present an adaptive “crystal growth” algorithm which is designed to assign a stencil \mathcal{S}_i^k from the smooth part of $f(x)$, if available, to all cells C_i^k which are themselves in the smooth part of $f(x)$. In this way a Gibbs-like phenomenon is avoided, and the resulting approximation is r th order accurate everywhere, except at cells which contain a discontinuity. This is accomplished by selecting the cell from the set of side-neighbors which minimizes the derivatives of the so-defined reconstruction.

We refer the reader to [1] for details of special essentially nonoscillatory (ENO) reconstruction techniques for triangulated meshes. Following the same principles, we present in Appendix A a simple technique to compute a “central” stencil that works on triangulated meshes. This central stencil is then used to define the polynomial $p_i^k(x; \mathcal{D}_k f)$ of (4.4) in section 5.

5. Numerical results. We have performed two kinds of numerical tests: for the point value discretization, we have tested the two methods of sections 3 and 4; for the cell average discretization, only the general method has been tested. In this case, we also compare our results with a multiresolution scheme where centered tensor product stencils and a regular grid diadic Cartesian grid is used.

As described in section 2, the method involve three steps: decoding, truncation, and encoding. The data v^L on the fine level are represented as follows:

$$Mv^L = (v^0, d^1, \dots, d^{L-1})^T,$$

where v^0 is the representation of v^L on the coarsest level and d^l are scale coefficients. In the truncation step, we truncate the scale coefficients according to

$$\tilde{d}_i^l = \begin{cases} 0 & \text{if } |d_i^l| \leq \epsilon_k, \\ d_i^l & \text{else.} \end{cases}$$

In the numerical experiments to follow, we take ϵ_k to be the following.

- For point values, $\epsilon_k = \epsilon$.
- For cell averages,

$$\epsilon_k = \alpha_k \epsilon_{k+1}$$

with α_k defined by

$$\alpha_k = \max_{C_i^k \in \mathcal{C}^k} \left\{ \sqrt{\frac{|C_j^{k+1}|}{|C_i^k|}}, \text{ where } C_i^k = \bigcup_{j \in I_i^k} C_j^{k+1} \right\},$$

that is, the maximum ratio of the area between a cell of level k and all the cells of level $k+1$ that have been agglomerated in it. For Cartesian grid, we take $\alpha_k = 2$.

We define the compression factor μ to be

$$\mu = \frac{N_L}{N_0 + |\{(i, l) \text{ such that } |d_i^l| > \epsilon_k\}|}.$$

We have performed numerical tests on two functions:

1. $f_1(x, y) = \cos 2\pi(x^2 + y^2)$ in $[0, 1]^2$,
2. f_2 , shown on Figure 5.1, is defined in $[-1, 1]^2$ by

$$\begin{aligned} &\text{if } x \leq \frac{1}{2} \cos(\pi y), \quad f_2(x, y) = u_{\sqrt{\pi/2}}(x, y), \\ &\text{if } x > \frac{1}{2} \cos(\pi y), \quad f_2(x, y) = u_{-\sqrt{\pi/2}}(x, y) + \cos(2\pi y), \end{aligned}$$

where u_ϕ is

$$\left. \begin{aligned} &\text{if } r \leq -\frac{1}{3}, \quad u_\phi(x, y) = -r \sin\left(\frac{\pi}{2}r^2\right), \\ &\text{if } r \geq \frac{1}{3}, \quad u_\phi(x, y) = 2r - 1 + \frac{1}{6} \sin(3\pi r), \\ &\text{if } |r| < \frac{1}{3}, \quad u_\phi(x, y) = |\sin(2\pi r)|, \end{aligned} \right\} \text{ where } r = x + \tan(\phi)y.$$

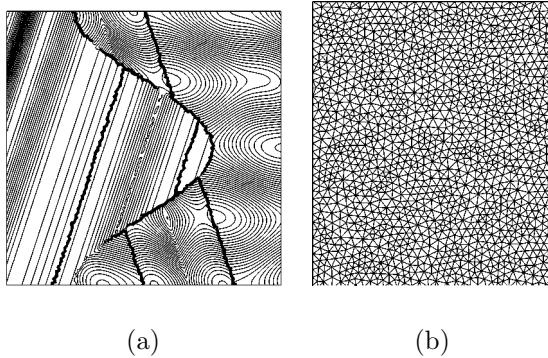


FIG. 5.1. (a) Isolines of f_2 ; (b) zoom of the upper left corner of the mesh.

5.1. Point value discretization. In a first example, the mesh has been obtained by refining four times a coarse mesh according to the procedure of Appendix A.1, with $n = 2$. It has 56,633 nodes and 112,384 triangles. The maximum radius of the triangles is $\rho \simeq 9 \cdot 10^{-3} \simeq 1/156$ and $J_L \simeq 240^2$. We use 3 levels. The results are displayed in Table 5.1. For comparison sake, we show in Table 5.2 results which are obtained from a Cartesian regular grid. From the approximation error point of view, we should consider the maximal radius. In this respect we have to compare to a grid of 156×156 . From the point of view of number of elements, we have to compare to a grid of 240×240 . Therefore we should compare these results to the entries for 128×128 and 256×256 in Table 5.2.

TABLE 5.1
Results for the refined grid.

Function	ϵ	μ	error (L^∞)
f_1	10^{-2}	57.43	$1.28 \cdot 10^{-2}$
	10^{-3}	25.08	$1.59 \cdot 10^{-3}$
	10^{-4}	5.85	$1.84 \cdot 10^{-4}$
f_2	10^{-2}	11.75	$1.54 \cdot 10^{-2}$
	10^{-3}	7.96	$1.63 \cdot 10^{-3}$
	10^{-4}	3.45	$1.71 \cdot 10^{-4}$

TABLE 5.2
Results for Cartesian grids, point value discretization.

Function	ϵ	64×64		128×128		256×256	
		μ	error (L^∞)	μ	error (L^∞)	μ	error (L^∞)
f_1	10^{-2}	7.37	$1.85 \cdot 10^{-2}$	29.04	$3.37 \cdot 10^{-2}$	115.3	$4.33 \cdot 10^{-2}$
	10^{-3}	1.94	$2.0 \cdot 10^{-3}$	7.06	$2.64 \cdot 10^{-3}$	28.02	$3.09 \cdot 10^{-3}$
	10^{-4}	1.11	$1.28 \cdot 10^{-4}$	1.83	$1.95 \cdot 10^{-4}$	6.9	$2.12 \cdot 10^{-4}$
f_2	10^{-2}	2.55	$2.34 \cdot 10^{-2}$	5.57	$3.70 \cdot 10^{-2}$	11.81	$4.6 \cdot 10^{-2}$
	10^{-3}	1.26	$1.27 \cdot 10^{-3}$	3.10	$1.61 \cdot 10^{-3}$	7.96	$2.54 \cdot 10^{-3}$
	10^{-4}	1.08	$9.75 \cdot 10^{-5}$	1.28	$1.50 \cdot 10^{-4}$	3.51	$1.80 \cdot 10^{-4}$

In a second example, we use a random mesh. The mesh generator ensures a certain regularity: the ratio of the circumcircle and the inner circle are controlled. Here three levels are used, with 12, 526, 2, 992, 706 nodes and 24, 650, 5, 782, and 1, 310 triangles, respectively. The results are displayed in Table 5.3. The maximum radius of the triangles of the finest level is $\simeq 1.8 \cdot 10^{-2} \simeq 1/55$ and $J_L \simeq 110^2$. From the approximation error point of view, we consider the maximal radius and therefore we have to compare to a grid of 55×55 . From the point of view of number of elements, we have to compare to a grid of 110×110 . Therefore, we should compare these results to the entries for 64×64 and 128×128 in Table 5.2.

These two examples, and many others that are not presented here indicate that the multiresolution analysis is stable. Furthermore, the MR scheme for the unstructured grid seems to be comparable in performance to corresponding Cartesian grids.

5.2. Cell-average discretization. In a first set of experiments, we have compared the compression and relative error for the functions f_1 and f_2 on $[-1, 1]^2$, our general agglomeration method to corresponding MR schemes for cell-average discretization on Cartesian grids. We start with a fine mesh which is generated from the triangulation of the previous example by finite element cells which are described as choice (c) in section 5.2.1; therefore, the number of cells is the same as the number of nodes in the triangulation, namely, $J_L = 12, 526$. It corresponds to $J_L \simeq 110^2$. The size of the maximal cell is of the order of $1/50$. Using five levels, the process of agglomeration generates successively 1, 980, 322, 57, and 11 cells. As in the previous example, this should be compared with Cartesian grids between 64×64 and 128×128 . The results are displayed in Table 5.4 (agglomeration procedure) and 5.5 (regular analysis).

As we can see, the compression factors are very similar for both methods. Figure 5.2 shows the multiresolution representation of f_2 (on a 512×512 mesh), and $\epsilon = 10^{-3}$.

The encoding/decoding procedure for the agglomeration procedure is illustrated on Figure 5.3. We analyze the same function, on the same mesh, with only three levels

TABLE 5.3
Results for the coarsening procedure.

Function	ϵ	μ	error (L^∞)
f_1	10^{-2}	16.03	$5.03 \cdot 10^{-2}$
	10^{-3}	5.43	$1.76 \cdot 10^{-3}$
	10^{-4}	1.50	$1.77 \cdot 10^{-4}$
f_2	10^{-2}	4.22	$1.23 \cdot 10^{-1}$
	10^{-3}	2.43	$2.29 \cdot 10^{-3}$
	10^{-4}	1.17	$1.36 \cdot 10^{-4}$

TABLE 5.4
Results for the agglomeration procedure.

Function	ϵ	μ	error (L^∞)	error (L^1)
f_1	10^{-2}	16.45	$7.75 \cdot 10^{-2}$	$5.37 \cdot 10^{-3}$
	10^{-3}	4.05	$3.06 \cdot 10^{-3}$	$4.46 \cdot 10^{-4}$
	10^{-4}	1.15	$2.98 \cdot 10^{-4}$	$1.61 \cdot 10^{-6}$
f_2	10^{-2}	2.85	$4.83 \cdot 10^{-2}$	$2.56 \cdot 10^{-3}$
	10^{-3}	1.71	$2.97 \cdot 10^{-3}$	$3.42 \cdot 10^{-4}$
	10^{-4}	1.02	$2.92 \cdot 10^{-4}$	$3.1 \cdot 10^{-6}$

TABLE 5.5
Results for Cartesian grid, cell average discretization.

Function	ϵ	64×64			128×128		
		μ	error (L^∞)	error (L^1)	μ	error (L^∞)	error (L^1)
f_1	10^{-2}	7.69	$8.9 \cdot 10^{-3}$	$1.75 \cdot 10^{-3}$	21.79	$6.57 \cdot 10^{-3}$	$1.14 \cdot 10^{-3}$
	10^{-3}	2.32	$1.11 \cdot 10^{-3}$	$2.29 \cdot 10^{-4}$	6.97	$8.99 \cdot 10^{-4}$	$1.75 \cdot 10^{-4}$
	10^{-4}	1.29	$9.20 \cdot 10^{-5}$	$1.66 \cdot 10^{-5}$	2.23	$1.09 \cdot 10^{-4}$	$2.19 \cdot 10^{-5}$
f_2	10^{-2}	2.45	$1.13 \cdot 10^{-2}$	$1.81 \cdot 10^{-3}$	4.74	$1.07 \cdot 10^{-2}$	$1.49 \cdot 10^{-3}$
	10^{-3}	1.38	$7.39 \cdot 10^{-4}$	$0.95 \cdot 10^{-4}$	3.00	$1.16 \cdot 10^{-3}$	$1.92 \cdot 10^{-4}$
	10^{-4}	1.09	$6.27 \cdot 10^{-5}$	$0.92 \cdot 10^{-5}$	1.52	$8.86 \cdot 10^{-5}$	$1.12 \cdot 10^{-5}$

this time. The first line of the figure (noted (a)) represents the effect of the decimation operator. One starts from the representation of f_2 on the fine level, then decimates and gets the figures medium-(a) and coarse-(a). The errors between two consecutive levels are plotted on the second line. For example, the first (b)-picture represents the (truncated) error between the (a)-fine plot and what is reconstructed from the (a)-medium plot. The third line represents what is obtained by reconstruction and correction with the truncated errors from the coarsest representation of f_2 , plotted on coarse-(c) and coarse-(a).

In a second set of experiments, we show all the advantages of using an unstructured mesh: the geometrical flexibility. The same functions are analyzed on a domain similar to a smiling face. Four levels are used. The mesh has 12,962 cells, the agglom-

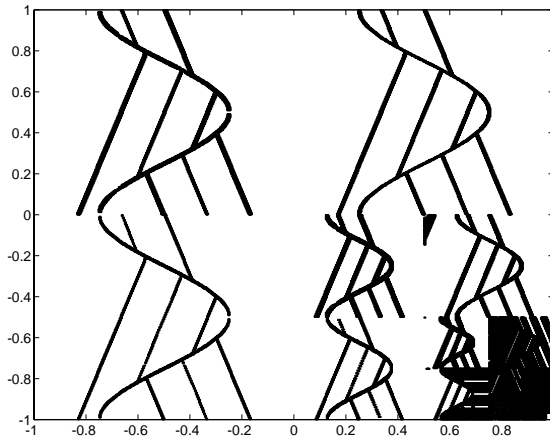


FIG. 5.2. Multiresolution representation of f_2 on a 512×512 mesh.

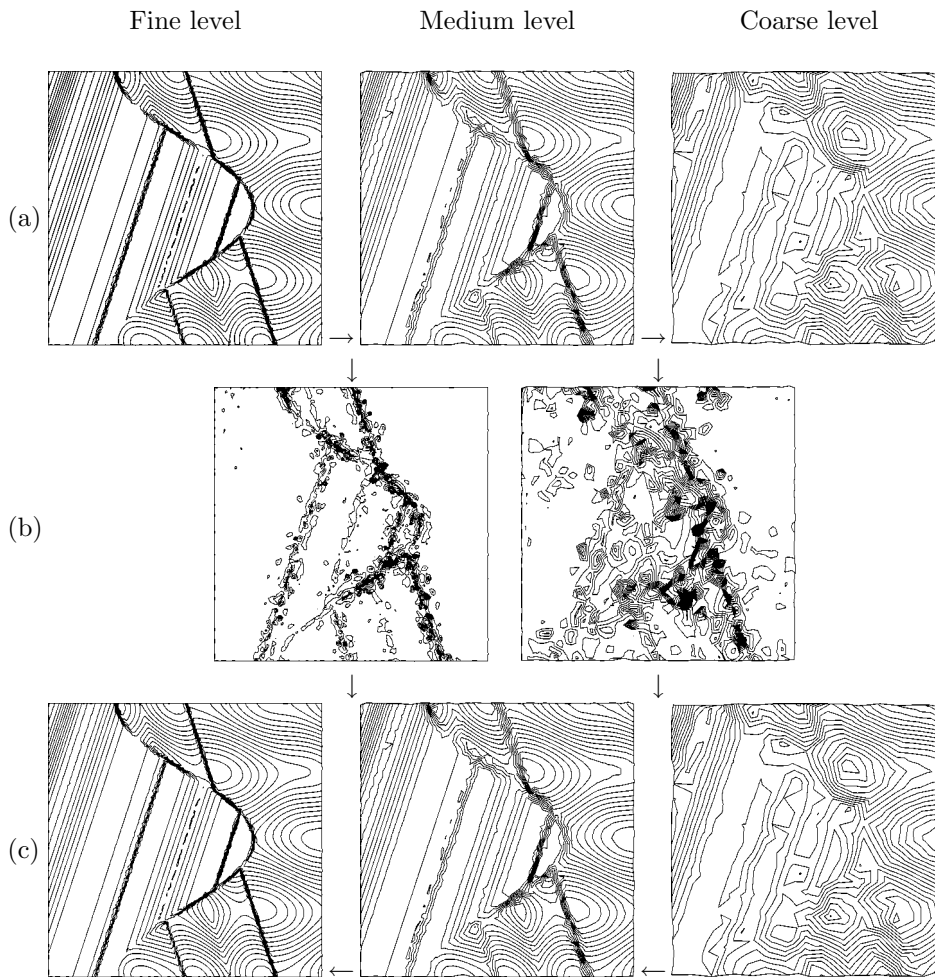


FIG. 5.3. *Encoding/decoding procedure: (a) Decimation, (b) truncated errors, (a) + (b) = decoding, (c) encoding.*

erated meshes have 2, 122, 369, and 68 cells. On Figure 5.4, we show the cells of the coarsest level. Some figures concerning f_2 are given. Figure 5.5 shows the encoded function on the first line. The coarsest level is plotted on the right, and the finest on the left. On the second line of Figure 5.5, we show the truncated errors.

Last, on Table 5.6, we give the compression factor and L^1 error for this particular domain.

6. Conclusions. In this paper, we have demonstrated the feasibility of designing MR schemes for discrete data which originate from discretizations by point values or cell-averages in unstructured meshes.

The main ingredient which is needed to accomplish this task is a reliable procedure to generate a nested sequence of discretization either by coarsening a given fine mesh, or by refining a given coarse mesh. The procedures that we used in this paper are probably far from being a final product, and they were used in order to explore the considerations associated with this problem.

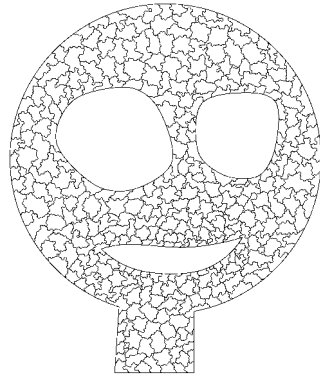


FIG. 5.4. *Agglomerated cells, third level.*

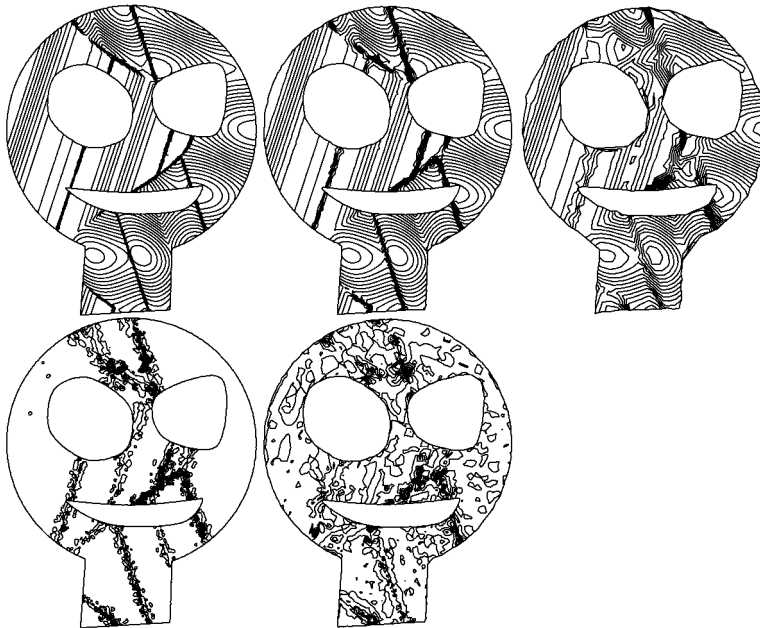


FIG. 5.5. *Reconstructed function and scale coefficients.*

Although the only theory which we can apply at this stage to the analysis of stability of the data compression algorithms is for hierarchic approximations, our numerical results indicate that the compression error is proportional to the tolerance ϵ with a constant which is of order 1, even for randomly generated meshes. The compression ratio, however, depends strongly on the “quality” of the mesh: since the scale coefficients are really approximation errors, their size depends on both the regularity of the function and the regularity of the grid.

We conclude that the main effect of lack of regularity of the mesh is on the rate of compression, and it does not seriously affect the compression error. However, we have not been able to quantify this conjecture yet.

Appendix A. Implementation. In this section, we show how to apply the general framework presented above to two kinds of representation of functions on un-

TABLE 5.6
Results for the agglomeration procedure on the domain with holes.

function	ϵ	μ	error (L^∞)	error (L^1)
f_1	10^{-2}	13.67	$2.21 \cdot 10^{-2}$	$1.11 \cdot 10^{-3}$
	10^{-3}	3.31	$8.67 \cdot 10^{-4}$	$1.04 \cdot 10^{-4}$
	10^{-4}	1.17	$7.05 \cdot 10^{-5}$	$3.37 \cdot 10^{-6}$
f_2	10^{-2}	2.65	$2.15 \cdot 10^{-2}$	$6.48 \cdot 10^{-4}$
	10^{-3}	1.50	$9.17 \cdot 10^{-4}$	$6.61 \cdot 10^{-5}$
	10^{-4}	1.02	$6.97 \cdot 10^{-5}$	$5.27 \cdot 10^{-7}$

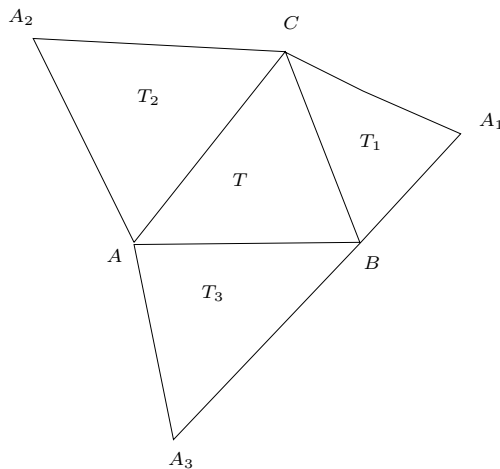


FIG. A.1.

structured meshes: point values and average values. In both cases, we describe the reconstruction operator. The most challenging task is the definition of the stencil on which the reconstruction relies. In order to simplify the discussion, we have limited ourselves to a *quadratic* reconstruction. We do not describe the procedures to eliminate points (in the case of the discretization by point values) or to agglomerate cells (in the case of the discretization by cell average). We have used exactly the same algorithms as for multigrid techniques; see [9, 16, 23] for details. When refinement is needed, we refine each triangle by adding the midpoint of the triangle edges.

We start with notations: let Ω be the computational domain, and assume that it is bounded. The set Ω is approximated by a polygon Ω^L which is triangulated; let \mathcal{T}^L denote the triangulation and let $X^L = \{M_i\}_{1 \leq i \leq J_L}$ denote its nodes. As before we denote by $k = L$ the finest level of resolution in the sequence and by $k = 0$ is the coarsest. In general we shall refer to the number of nodes by n_s and to the number of triangles by n_t .

A.1. Discretization by point values. For the purpose of MR one needs a right-inverse to \mathcal{D}_k . Here it is the Lagrange interpolation which is uniquely defined once we provide the stencils \mathcal{S}_i^k in (3.6). In order to simplify the presentation, we describe only what can be done for a third order interpolation. At the end of this paragraph, we indicate how this can be extended to more general situations.

In order to define the stencils, we have chosen a rather heuristic approach. We consider a triangulation \mathcal{T} , and let T be any of its triangles.

We first assume that T is an interior triangle; i.e., none of its edges are on the boundary. Then there exists a triangle on the other side of each side of T , namely, T_1, T_2, T_3 (Figure A.1), which we refer to as side-neighbors. The set of all the vertices of T, T_1, T_2, T_3 has six elements. In general, this set is not geometrically degenerate; i.e., there is a unique solution to the Lagrange interpolation problem. It would not be the case if these points were on a conic.

Now, if T is on the boundary, we may make a similar construction in general. If not, T certainly belongs to a family of triangles assigned to a triangle T' as in the previous discussion. We assign to T the stencil constructed for T' . In all the practical examples we have considered, this has been enough. However, we are very well aware that counterexamples can be constructed, and additional heuristics must be added in these special cases.

Let us mention that this method of constructing stencils can be generalized to higher degree polynomials; for example, see [1].

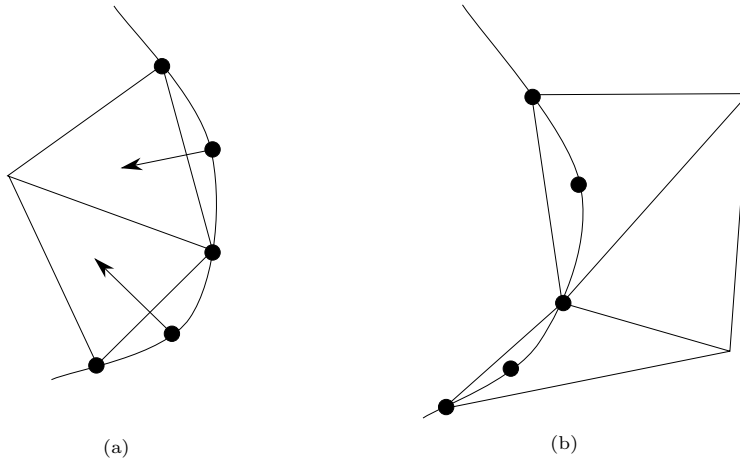


FIG. A.2. (a) Convex boundary and (b) concave boundary.

In all cases, the stencil is used to have an approximation in T . Depending on the local concavity of the boundary, it is possible for some points of \mathcal{T}^k to be in the exterior of the coarser triangulation \mathcal{T}^{k-1} ; see Figure A.2. Note that this does not contradict the requirement of nestedness. In this case, we predict the corresponding values by extrapolation from the closest triangle in \mathcal{T}^{k-1} .

A.2. Discretization by cell average. In this section, we assume that we are given a partition of Ω by disjoint cells $\mathcal{C}^L = \{C_i^L\}_{i=1}^{J_L}$ such that

$$(A.1) \quad \Omega^L =: \overline{\cup_{i=1}^{J_L} C_i^L} \subseteq \Omega, \quad C_i^L \cap C_j^L = \emptyset \text{ for } i \neq j.$$

The decimation and prediction operators are defined in section 4. We provide here a description of a procedure to assign the stencil \mathcal{S}_i^k to the cell C_i^k for a quadratic reconstruction as defined by (4.3)–(4.5). For the sake of clarity, we give the details of the case $r = 3$ which corresponds to piecewise-quadratic reconstruction, though a more general discussion can be given.

We follow the procedure of subsection A.1. For that, we identify each of the cells C_i^k with a point which we take to be the centroid of C_i^k (even though it may not belong to C_i^k). For this set of points we construct a triangulation T' , here a

Delaunay mesh. It is clear that some constraints, coming from the geometry of the problem have to be added. The most obvious constraint is that two cells that are not close (because they are separated by a hole) should not be connected (see Figure A.3). We decide that a triangle is inadmissible if its centroid does not belong to the fine triangulation \mathcal{T}^L . For example, in Figure A.3 the exact domain is inside

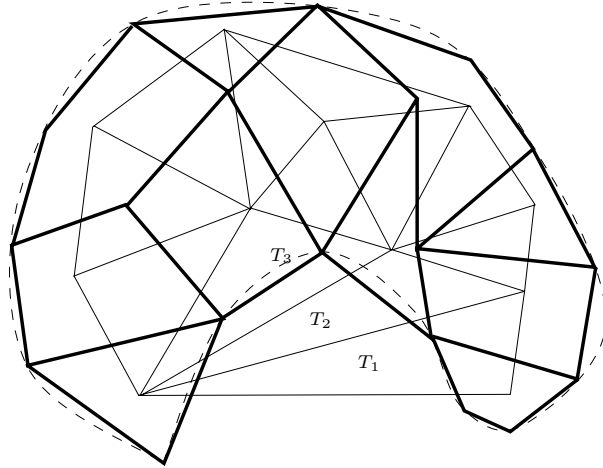


FIG. A.3.

the dotted line. The partition is made of the cells which are bounded by the thick lines. The corresponding triangulation of these cells is represented by the thin lines. The triangles T_1 and T_2 are not accepted because their centroid is outside of the computational domain, while T_3 is accepted. Another constraint is that the accepted triangles should not be too flat. This case may be encountered at an almost flat boundary. The boundary triangles are tested as follows: we consider all the boundary points of \mathcal{T}'_l . For any of these points we consider the triangles having it as vertex. We compute the average ratio $(\frac{h}{\rho})_{av}$ of its circumcircle and its inner circle. If this ratio for a boundary triangle is too far from the average one,

$$\left| 1 - \frac{h/\rho}{(h/\rho)_{av}} \right| > \delta,$$

we remove this triangle. We have chosen $\delta = 0.1$. This choice of stencil is so that this reconstruction procedure is not hierarchical in general.

Appendix B. Stability analysis and existence of MR bases. We assume that the sequence $\{\mathcal{R}_k \mathcal{D}_k\}_{k=0}^\infty$,

$$(B.1) \quad (\mathcal{R}_k \mathcal{D}_k) : \mathcal{F} \rightarrow \mathcal{F},$$

is a sequence of (discrete) approximation in the Banach space \mathcal{F} , i.e., that for any $f \in \mathcal{F}$,

(i)

$$(B.2) \quad \|\mathcal{R}_k \mathcal{D}_k f\| \leq C_A^k \|f\|,$$

(ii)

$$(B.3) \quad \|\mathcal{R}_k \mathcal{D}_k f - f\| \rightarrow 0 \quad \text{as } k \rightarrow \infty.$$

Using the principle of uniform boundedness we conclude that there exists a constant C_A such that for all k

$$(B.4) \quad C_A^k \leq C_A.$$

If (B.1) is a *nested* sequence of discretization, we get that the direct MR transform (2.8) is stable with respect to perturbations in the input data v^L and that

$$(B.5) \quad \begin{aligned} \langle \delta(d^k) \rangle_k &= |\delta(e^k)|_k \leq C_A(1 + C_A)|\delta(v^L)|_L, \\ |\delta(v^0)|_0 &\leq C_A|\delta(v^L)|_L, \end{aligned}$$

where $\delta(\cdot)$ denotes the perturbation, and the discrete norms above are defined as follows:

$$(B.6) \quad |v^k|_k = \|\mathcal{R}_k v^k\| ;$$

$$(B.7) \quad \langle d^k \rangle_k = |E_k d^k|_k .$$

In the case of point value discretization we consider the sequence $\{\mathcal{I}^k(x; \mathcal{D}_k f)\}_{k=0}^\infty$ in the Banach space which consists of continuous functions in Ω with the maximum norm

$$(B.8) \quad \|f\| = \|f\|_\infty =: \max_{x \in \Omega} |f(x)|.$$

The conditions (B.2) and (B.3), which are required of a sequence of approximation in this space, state that for any f which is continuous in Ω

$$(B.9) \quad \max_{x \in \Omega} |\mathcal{I}^k(x; \mathcal{D}_k f)| \leq C_A^k \cdot \max_{x \in \Omega} |f(x)|,$$

and

$$(B.10) \quad \lim_{k \rightarrow \infty} \max_{x \in \Omega} |\mathcal{I}^k(x; \mathcal{D}_k f) - f(x)| = 0.$$

The “natural” function space for cell-average discretization is $\mathcal{F} = L_1(\Omega)$, and there (B.2)–(B.3) take the following form:

$$(B.11) \quad \int_\Omega |(\mathcal{R}_k \mathcal{D}_k f)(x)| dx \leq C_A^k \int_\Omega |f(x)| dx,$$

$$(B.12) \quad \lim_{k \rightarrow \infty} \int_\Omega |(\mathcal{R}_k \mathcal{D}_k f)(x) - f(x)| dx = 0.$$

Experimentally, we have seen that these conditions (B.9), (B.11), (B.10), (B.12) seem true when the stencil needed to define \mathcal{I}^k is not too distorted but also if the size of consecutive stencils for consecutive levels grow smoothly, say at most as a geometrical progression. If the first condition is well known to ensure convergence at fixed levels, the second one, even though stated here in a rather vague fashion, seems to ensure the stability through scales. Some indications towards this are given in [1].

In [13] we investigate the stability of the inverse MR transform and the related question of existence of MR bases for mappings in \mathcal{F} .

Acknowledgments. We acknowledge the referees for their very constructive comments.

REFERENCES

- [1] R. ABGRALL, *Design of an Essentially Nonoscillatory Reconstruction Procedure on Finite Element Type Meshes*, Tech. Report 91-84, Institute for Computer Applications in Science and Engineering, Hampton, VA, 1991; in revised form as INRIA Tech. Report 1592, February 1992.
- [2] R. ABGRALL, *Multiresolution analysis on unstructured meshes: Application to CFD*, in Numerical Methods for Fluid Dynamics, Vol. V, K. Morton and M. Baines, eds., Oxford Science Publications, 1995, pp 271–276.
- [3] R. ABGRALL AND A. HARTEN, *Multiresolution Representation in Unstructured Meshes: Preliminary Report*, Tech. Report 94–20, Computational and Applied Math., UCLA, Los Angeles, CA, 1994.
- [4] G. BEYLKIN, R. COIFMAN, AND V. ROKHLIN, *Fast wavelet transform and numerical algorithms. I*, Comm. Pure Appl. Math., 44 (1991), pp. 141–183.
- [5] B. BIHARI AND A. HARTEN, *Multiresolution Schemes for the Numerical Solution of 2-D Conservation Laws*, Tech. Report, University of California, Los Angeles, CA, June 1994.
- [6] B. BIHARI AND A. HARTEN, *Application of generalized wavelets: An adaptive multiresolution scheme*, J. Comput. Appl. Math., 61 (1995), pp. 275–321.
- [7] A. COHEN, I. DAUBECHIES, AND J.-C. FEAUVEAU, *Biorthogonal bases of compactly supported wavelets*, Comm. Pure Appl. Math., 45 (1992), pp. 485–560.
- [8] I. DAUBECHIES, *Orthonormal bases of compactly supported wavelets*, Comm. Pure Appl. Math., 41 (1988), pp. 909–996.
- [9] H. GUILLARD, *Node-nested Multigrid Method with Delaunay Coarsening*, Tech. Report 1898, INRIA, May 1993.
- [10] A. HARTEN, *Discrete multiresolution analysis and generalized wavelets*, Appl. Numer. Math., 12 (1993), pp. 153–192.
- [11] A. HARTEN, *Adaptive multiresolution schemes for shock computations*, J. Comp. Phys., 115 (1994), pp. 319–338.
- [12] A. HARTEN, *Multiresolution algorithms for the numerical solution of hyperbolic conservation laws*, Comm. Pure Appl. Math., 48 (1995), pp. 1305–1342.
- [13] A. HARTEN, *Multiresolution representation of data: A general framework*, SIAM J. Numer. Anal., 33 (1996), pp. 1205–1256.
- [14] A. HARTEN AND S. R. CHAKRAVARTHY, *Multi-dimensional Eno Schemes for General Geometries*, Tech. Report 91-76, Institute for Computer Applications in Science and Engineering, Hampton, VA, September 1991.
- [15] A. HARTEN AND I. YAD-SHALOM, *Fast multiresolution algorithms for matrix-vector multiplication*, SIAM J. Numer. Anal., 31 (1994), pp. 1191–1218.
- [16] M.-H. LALLEMAND, H. STEVE, AND A. DERVIEUX, *Unstructured multigriding by volume agglomeration: Current status*, Comput. & Fluids, 21 (1992), pp. 397–433.
- [17] S. MALLAT, *Multiresolution approximation and wavelets orthonormal bases of $L^2(\mathbb{R})$* , Trans. Amer. Math. Soc., 315 (1989), pp. 69–87.
- [18] Y. MEYER, *Ondelettes et Opérateurs*, Hermann, Paris, 1990.
- [19] P. OSWALD AND R. LORENZ, *Multilevel finite element Riesz bases in Sobolev spaces*, in Proc. 9th Conference on Domain Decomposition, Ullensvang, Norway, June 1996.
- [20] P. SCHODER AND W. SWELDENS, *Spherical wavelets: Efficiently representing functions on the sphere*, in Computer Graphics Proceedings, Annual Conference Series, 1995.
- [21] R. STEVENSON, *Piecewise Linear Pre-Wavelets on Non-Uniform Meshes*, Tech. Report 9701, Univ. of Nijmegen, The Netherlands.
- [22] W. SWELDENS, *The lifting scheme: A custom-design construction of biorthogonal wavelets*, Appl. Comp. Harm. Anal., 3 (1996), pp. 186–200.
- [23] V. VENKATAKRISHNAN AND D. MAVRIPLIS, *Agglomeration multigrid for the three-dimensional Euler equations*, AIAA J., 33 (1995).